AIAA 81-1967R

Sound Propagation Through a Variable Area Duct: Experiment and Theory

Richard J. Silcox* and Harold C. Lester†
NASA Langley Research Center, Hampton, Virginia

A comparison of experiment and theory has been made for the propagation of sound through a variable area axisymmetric duct with zero mean flow. Measurement of the acoustic pressure field on both sides of the constricted test section was resolved on a modal basis for various spinning mode sources. Transmitted and reflected modal amplitudes and phase angles were compared with finite-element computations. Good agreement between experiment and computation was obtained over a wide range of frequencies and modal transmission through a variable area duct was found to be governed by the throat modal cut-off ratio.

Nomenclature

$A^{\pm}_{mn}$ = complex modal amplitude coefficients, Eq. (2)
a = radius of uniform duct section, 0.15 m
B_n = source modal amplitude coefficient, Eq. (11)
c_0 = ambient speed of sound
J_m = Bessel function of first kind and order m
j = $\sqrt{-1}$
k = ω/c_0
ka = frequency parameter
M = maximum value of m
(m,n) = (azimuthal, radial) mode indices
N = maximum value of n
$P^{\pm}_{mn}$ = acoustic pressure coefficient, Eq. (8)
p = acoustic pressure, Eq. (2)
r,θ,x = cylindrical coordinates
t = time
u,v,w = acoustic particle velocities in x,r,θ directions, respectively
ζ_T = termination impedance, Eq. (12)
λ_{mn} = hard wall radial eigenvalues such that $J'_m(\lambda_{mn}a)=0$
ξ = cut-off ratio, Eq. (13)
ρ_0 = ambient density
ϕ_n = source modal phase, Eq. (11)
$\Omega^{\pm}_{mn}$ = modal propagation constants, Eq. (3)
ω = circular frequency

Introduction

In recent years a considerable amount of research has been directed toward developing analytical methods and numerical procedures for modeling the propagation of sound in variable area ducts. One of the primary goals of this research is to understand and utilize the sound attenuation produced by near sonic or high Mach number inlets. This concept, when used in combination with an effective acoustic liner, has the potential of significantly quieting present generation aircraft engines. These analyses include detailed modeling of: arbitrary axisymmetric area variations, axial gradients of compressible mean flows, realistic boundary-layer profiles, and arbitrary acoustic excitations. The solution techniques include purely analytical procedures,[1,2] basis function expansions,[3,4] and completely numerical schemes.[5-7] However, little reliable experimental data have become available against which these analyses can be verified. An exception is the work of Nayfeh et al.[8] in which he compared theory and experiment for higher-order azimuthal modes. His analysis, however, precluded cases of modes near cut-on due to reflections and cross modal coupling effects. A comparison of finite-element and finite-difference solutions with some preliminary NASA Lewis test data was also reported by Baumeister in Ref. 9.

In response to this need for a definitive experimental data base, a research investigation has been initiated to determine the transmission characteristics of higher-order acoustic modes in a variable area duct. This work is part of an ongoing effort to understand the basic suppression mechanism of high Mach number, aircraft engine inlets. A unique feature of the research study is the use of the NASA Langley spinning mode synthesizer to generate individually dominant azimuthal mode patterns.

This paper deals with the propagation of sound through a variable area duct in the absence of flow. The effects of flow will be reported in a later paper. The constriction geometry used for these tests consisted of identical conical contraction and expansion sections with a wall slope of 3.6 deg. The area ratio was approximately 2 over a length of 10 duct radii. Source pressure distributions, with a single dominant azimuthal mode, were generated over a wide range of frequencies for the $m=1$ and 2 azimuthal spinning modes. Transmission and reflection coefficients derived from measured data were compared to calculations made by the finite-element algorithm of Ref. 6. Modal coefficients from measured and calculated data were obtained by both Fourier and Fourier-Bessel transforms and a least-square-fit procedure.

Experiment Setup and Measurement Procedure

The experiment was conducted in the spinning mode synthesizer (SMS)/flow duct facility of the NASA Langley Aircraft Noise Reduction Laboratory. This facility provides a controlled acoustic environment for studying the propagation characteristics of dominant azimuthal (spinning) mode pressure distributions in flows up to Mach numbers of about 0.6. For the experiment reported in this paper, the facility was used to study the transmission and reflection properties of the $m=1$ and 2 azimuthal modes propagating through a variable area test section in the absence of flow.

Geometry

Figure 1 is a photograph of the SMS/flow duct facility. Details can be obtained from Fig. 2 which is a schematic of the test setup. The facility was constructed to permit precisely measured acoustic data to be obtained on either side (positions A and B on the source side and positions C, D, and E on the transmission side of Fig. 2) of a variable area test section. In this case the test section has an area ratio of 2.0. The wall contour consists of two conical sections of half-angle

Presented as Paper 81-1967 at the AIAA 7th Aeroacoustics Conference, Palo Alto, Calif., Oct. 5-7, 1981; submitted Oct. 22, 1981; revision received Feb. 26, 1982. This paper is declared a work of the U.S. Government and therefore is in the public domain.

*Aerospace Engineer, Noise Control Branch, ANRD. Member AIAA.
†Aerospace Engineer, Noise Control Branch, ANRD.

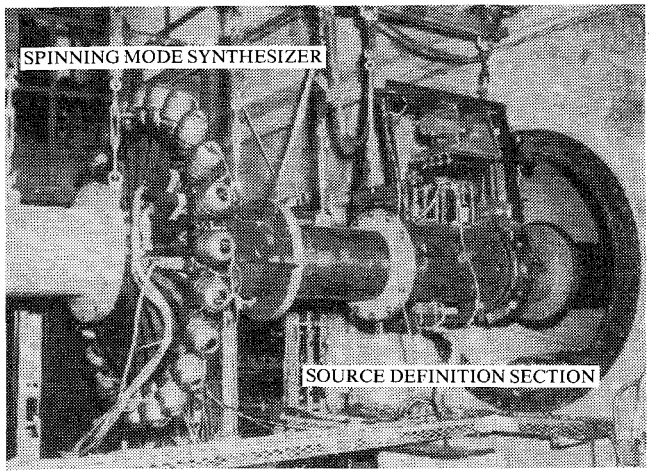

Fig. 1 Flow duct facility with SMS and source measurement apparatus.

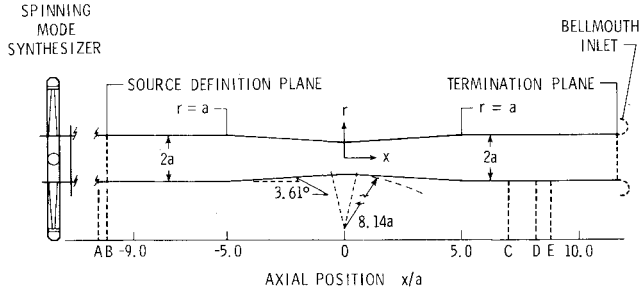

Fig. 2 Schematic of test setup.

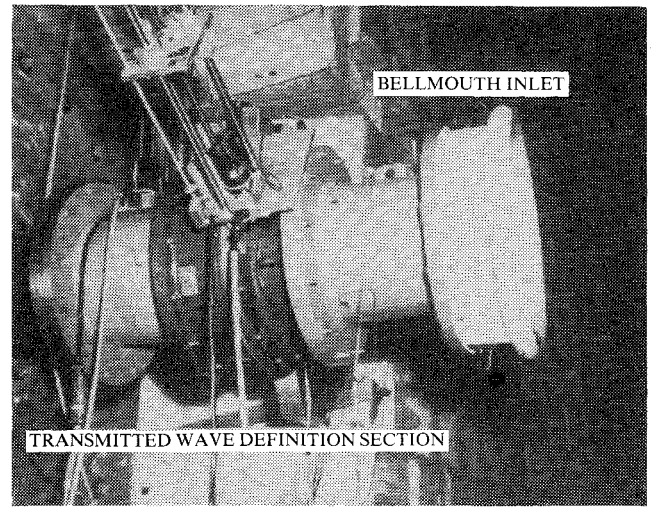

Fig. 3 Transmitted wave measurement apparatus and duct termination.

Table 1 Measurement stations and functions

Measurement station	x/a	Measurement $p(r,\theta,x)$
A	−10.51	$p(r,\theta,-10.51)$
B	−10.09	$p(r,\theta,-10.09)$
C	7.01	$p(r,-1.4\text{ deg},7.01)$
D	8.15	$p(1.0,\theta,8.15)$
E	8.80	$p(r,59.0,8.8)$

3.61 deg faired at the throat ($x=0$) by a circular arc of $9.14a$ ($a=0.15$ m). This faired arc section extends $0.512a$ on either side of the throat and joins smoothly with the conical sections. The variable area section is symmetric about the throat and is of length $10a$. The test section is joined on either end to uniform circular ducts which contain the measurement sections.

The equations describing the wall contour geometry are as follows.

$$r/a = 8.843 - [66.3 - (x/a)^2]^{1/2} \qquad |x/a| \le 0.512$$

$$= 0.717 + [\,|x/a| - 0.512]\tan 3.608\text{ deg} \qquad 0.512 \le |x/a| \le 5.0$$

$$= 1.0 \qquad 5.0 \le |x/a| \le 11.62 \qquad (1)$$

Data Acquisition Method

Pressure measurements were recorded at acquisition positions A-E shown in Fig. 2. Position A, at the left end of the test setup, is located far enough from the SMS (acoustic source) to allow a nonpropagating mode to attenuate before reaching this source definition section. At the opposite end, terminating the duct, is a bellmouth inlet (Fig. 3) from which the sound radiates into an anechoic chamber. The termination characteristics of this inlet are documented in Ref. 10. In addition, due to the forward-backward wave separation techniques employed in this experiment, the reflected waves from the inlet may be separated from the transmitted wave propagating through the constriction.

Measurement positions A and B (Fig. 1) comprise the source definition section of the duct with B the reference position $-10.09a$ from the constriction throat. It is at these two axial positions that pressure measurements are made (Table 1) defining the incident and reflected pressure waves on a mode by mode basis. The modal decomposition technique employed here utilizes a Fourier and Fourier-Bessel transform technique to reduce pressure data taken at $2M$ azimuthal positions and N radial positions, where $(\pm M,N)$ are the maximum azimuthal mode and radial mode indices, respectively. This produces $N(2M+1)$ unknown modal coefficients to be resolved. This is to say, data at planes A and B are taken at N common radial positions on each of $2M$ radial lines from the duct center to the outer wall equispaced about the circumference. The data reduction technique will be described in a later section.

Measurement locations C, D, and E of Fig. 2 comprise the transmitted wave measurement section (Fig. 3) with location D being the reference position (Table 1). Measurement stations C and E consist of diameter traverses at fixed azimuthal positions of −1.4 and 59.0 deg, respectively, and axial positions are as given in the table. Station D is an array of four flush-mounted wall microphones spaced 90 deg apart in the axial plane $8.15a$ from the throat. These microphones may be rotated through 90 deg such that the pressure at any azimuthal position on the wall may be recorded. In combination, these three measurement stations provide data for another modal decomposition technique, based on a least-squares-solution technique.

The data acquisition system for the eight measurement microphones at stations A-E is shown schematically in Fig. 4. The microphones are ceramic transducers with a 0.8-mm sensor element diameter. They were amplitude and phase calibrated vs frequency against a common condenser microphone and checked each day for amplitude drift. The radial traversing probes consisted of the aforementioned microphones potted into the end of 6.35-mm-diam tubes with the sensor element flush with the end of the probes. As shown in the block diagram, the microphones are multiplexed into a single analog channel. A programmable gain amplifier sets the gain for optimum signal resolution for the selected transducer and the signal is filtered by a 100-Hz bandwidth tracking filter. The digitizing process is performed using a 12-bit analog-to-digital system utilizing a trigger to initialize data acquisition always at the same point on the rising side of the

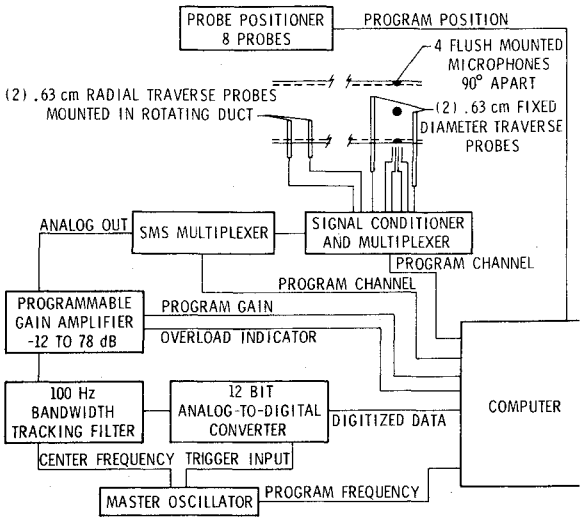

Fig. 4 Data acquisition system.

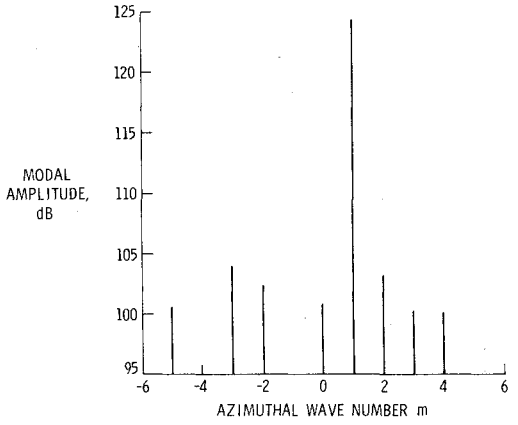

Fig. 5 Typical source azimuthal wave spectra, $ka=5.04$, for (1,0) mode.

oscillator excitation signal that drives both the trigger input and the SMS acoustic drivers. This technique provides phase averaging of the microphone signals and a common reference phase for all microphone measurements. The final averaged digitized data are then curve fit, using a least-square technique, to a sine wave of arbitrary amplitude, phase and offset, but of the source driving frequency. This results in a reliable measure of the amplitude and relative phase of each microphone. More details of this acquisition system are reported in Ref. 10.

Mode Generation

The spinning mode synthesizer (Fig. 1) is an acoustic source capable of generating arbitrary combinations of acoustic sound patterns at a specified frequency in the presence of airflow in a 0.3-m-diam duct. Specified duct modes are generated by controlling the amplitude and phase of 24 acoustic drivers equispaced around the duct wall in a plane perpendicular to the duct centerline. By properly adjusting the driver inputs individual spinning modes, combinations of modes or circumferential standing waves may be generated in the duct. Figure 5 shows a typical azimuthal wavenumber spectra generated by the synthesizer for a frequency parameter of $ka=5.04$. The desired first-order azimuthal mode dominates the acoustic field by 20 dB. A more detailed description of this facility may be found in Ref. 10.

Mode Decomposition Techniques

Two modal decomposition techniques were developed for application to the measured acoustic pressure data. The first is based on classical Fourier and Fourier-Bessel transforms and the second employs a least-squares data fit. It will be assumed in the discussions to follow, that the measured complex pressures (amplitude and phase) are satisfactory representations of the real acoustic pressure that exists at each particular position. The measurement of pressure was achieved as discussed previously and positioning accuracy was checked for each probe to better than 0.2-mm linear accuracy and 0.25 deg in angular position.

Transform Method

This model decomposition technique is similar to the methods proposed by Moore[11] and Kraft et al.[12] The method utilizes the orthogonal characteristics of the hardwall circular duct eigenfunctions which describe the pressure field at any location in the duct as follows.

$$p(r,\theta,x)=\sum_m\sum_n[A^+_{mn}e^{j\Omega^+_{mn}x}+A^-_{mn}e^{j\Omega^-_{mn}x}]J_m(\lambda_{mn}r)e^{j(m\theta-\omega t)} \tag{2}$$

This represents a steady-state solution with an $e^{-j\omega t}$ harmonic time dependence. Here, m represents the azimuthal wavenumber (..., -3, -2, -1, 0, 1, 2, 3, ...). J_m is the Bessel function of the first kind of order m and λ_{mn} represents the solutions of the equations $J'_m(\lambda a)=0$, that is, the hardwall duct eigenvalues. The axial wavenumber is given by

$$\Omega^\pm_{mn}=\pm[k^2-\lambda^2_{mn}]^{1/2} \tag{3}$$

where $k=\omega/c_0$ is the total wavenumber. The modal coefficients $A^\pm_{mn}$ are unknown and are to be determined.

If the $e^{-j\omega t}$ factor is removed and both sides of Eq. (1) are multiplied by $e^{-jm'\theta}$ and integrated over the interval 0 to 2π, it becomes

$$\int_0^{2\pi}p(r,\theta,x)e^{-jm'\theta}d\theta=2\pi\sum_n[A^+_{m'n}e^{j\Omega^+_{m'n}x}+A^-_{m'n}e^{j\Omega^-_{m'n}x}]J_{m'}(\lambda_{m'n}r) \tag{4}$$

due to the orthogonal nature of the $e^{jm\theta}$ function. Applying a Fourier-Bessel transform to Eq. (4) results in

$$2\pi C_{m'n'}[A^+_{m'n'}e^{j\Omega^+_{m'n'}x}+A^-_{m'n'}e^{j\Omega^-_{m'n'}x}]=\int_0^a\int_0^{2\pi}re^{-jm'\theta}J_{m'}(\lambda_{m'n'}r)p(r,\theta,x)d\theta dr \tag{5}$$

due to the orthogonal nature of the Bessel function, where

$$C_{m'n'}=\frac{1}{2\lambda^2_{m'n'}}[(\lambda^2_{m'n'}a^2-m'^2)J^2_{m'}(\lambda_{m'n'}a)] \tag{6}$$

Equation (5), after the integrations on the right side are performed, is merely an algebraic equation for A^+_{mn} and A^-_{mn}. If the integrations of the right side are evaluated at two axial locations the modal coefficients may be determined.

The integration of the acoustic field in the azimuthal plane is essentially the Fourier transformation of the spatial pressure distribution to an azimuthal wavenumber spectra. Proper resolution of this function requires that there be a minimum of $2M$ equispaced azimuthal pressure measurements at each radial position, where M is the highest azimuthal mode number considered. In each case evaluated for this test, all the propagating azimuthal mode orders in the constant area duct were considered in the analysis. For the radial integration, ten radial pressure measurements were fit with a cubic spline routine. This representation was then used in the evaluation of the numerical integration of Eq. (5) in the

radial direction. This yields radial mode orders up to $n=9$, which was always well above any propagating mode orders.

Least-Squares Solution

An alternative method for determining the unknown modal coefficients from measured pressure data is by means of a least-squares technique. Such an approach can be used with overdetermined systems of simultaneous equations, that is, where there are more equations (pressures) than unknowns (modal coefficients).

As before, the pressure at a fixed location (r,θ,x) is given by Eq. (2). A similar series can be written for every pressure measurement location. This produces a set of simultaneous linear algebraic equations in the unknown modal coefficients as follows.

$$[E(P^{\pm}_{mn})]_{NP\times NA}\{A^{\pm}_{mn}\}_{NA\times 1}=\{P\}_{NP\times 1} \tag{7}$$

Here $\{P\}$ is a column vector of order NP of the measured (known) pressures and $\{A\}$ a column vector of order NA of the unknown modal coefficients. The $NP\times NA$ matrix possesses elements $P^{\pm}_{mn}$ where

$$P^{\pm}_{mn}=e^{jm\theta}e^{j\Omega^{\pm}_{mn}x}J_m(\lambda_{mn}r) \tag{8}$$

Each of the NP rows in Eq. (7) represents the series for a particular pressure measurement location. In general $NP>NA$, that is, there are more known measured pressures than unknown modal coefficients and the system (Eq. 7) is said to be overdetermined. In the present paper Eq. (7) was solved in the least-squares sense using a standard NASA Langley computer library subroutine.[13] The numerical procedure is based on finding the singular value decomposition of the matrix E (see, for example, Ref. 14).

Experimentally 80-120 pressure measurements were taken as input to this modal decomposition program. Forty of these points were always taken on the azimuthal traverse (station D) and 20-40 measurements were taken on each of the diameter traverses (stations C and E). The number depended on the complexity of the acoustic field and the number of modes to be considered.

Evaluation of Techniques

Both modal decomposition techniques were evaluated extensively using theoretically derived pressures (Eq. 2) computed at locations representative of each measurement section (see Table 1). These numerical tests indicate that computed pressure fields accurate to 0.1 dB in sound pressure level and 0.1 deg in phase can be analyzed using both decomposition techniques to reproduce modal coefficients to within the same accuracy. Spurious modes also arise from the decompositions. However, their amplitudes are usually 60-80 dB down in SPL and arise from truncation and numerical integration errors. If larger errors in the theoretically derived pressure field are introduced, a number of problems with the analysis programs appears. These problems were examined by introducing a Gaussian distributed random error into the computed pressure field. Typically the errors introduced had standard deviations of 1 dB in sound pressure level and 10 deg in phase.

Data with these characteristic errors demonstrate different limitations for each of the modal decomposition techniques. In the transform method, as long as the proper sampling criteria are met as specified previously, the solution yielded modal coefficients accurate to within the standard deviation (1 dB in SPL and 10 deg in phase) of the data for the dominant modes. However, the spurious mode coefficients (modes not used in generating the pressure field) took on significant nonzero values, 20-40 dB below the dominant modes depending on the relative magnitude of the dominant modes input. For example, a dominant (1,0) mode with a forward traveling wave amplitude of 100 dB and backward traveling wave amplitude of 80 dB, with the error just described introduced in the pressure field, would be recovered as a forward traveling (1,0) mode coefficient of 100 dB $\pm$ 1 dB and a backward traveling mode coefficient of 80 dB $\pm$ 1 dB. The spurious mode coefficients (i.e., $m=\ldots,-3,-2,-1,0,2,3,\ldots$ and $n=0,1,2,\ldots$) may range in amplitude roughly from 0 to 60 dB. The simulated experimental errors produce the spurious mode coefficients because the analysis attempts to recreate the pressure field exactly. However, due to its random nature a great deal of this error integrates to zero in the analysis and accounts for the relatively good solutions. It is for this reason that sources of systematic errors must be minimized. Errors of this type will tend to give rise to erroneous mode results such as incorrectly large or small reflection coefficients for calibration errors between adjacent microphones. For this reason microphone calibrations were performed both in amplitude and phase. Amplitude calibrations were checked daily and the positioning of each probe was carefully verified. In addition, intrusive probes were inserted within the cross section of the duct one at a time to prevent scattering from other probes.

These same errors when used to test the least-squares analysis showed similar sensitivities in general. One major additional limitation results from the restrictive sampling positions available (stations C, D, and E of Table 1). Numerical tests showed that if an excessive number of modes are considered in the least-squares analysis, spurious modes may dominate the solution due to the pressure field being nonunique at the limited pressure measurement locations. High amplitude azimuthal and axial standing wave solutions can yield residuals in the least-squares sense that are smaller than the known correct solution. This problem is aggravated by allowing more degrees of freedom (more unknown mode coefficients) in the solution or greater uncertainty in the pressure measurements. For pressure fields accurate to 0.1 dB in SPL and 0.1 deg in phase, this problem did not occur for the degrees of freedom examined. This problem, then, is considered to be related to the limited spatial positioning available rather than the solution technique itself. However, for the purposes of this experiment, care was exercised in selecting the set of unknown azimuthal and radial mode coefficients. The spinning mode synthesizer itself, with the capability of producing individually dominant azimuthal mode numbers, helped to overcome this problem along with a careful examination of the data collected at stations C, D, and E of Fig. 2. For higher frequencies, especially where the reflected wave was strong, a higher degree of uncertainty in defining the transmitted wave structure results.

Additional checks on the consistency of data between measurement stations were also made. This consisted of propagating plane waves and highly cut-on azimuthal modes through the constriction. Predictions showed these cases to be minimally affected by the geometry change. Table 2 shows the results of these experiments. Since the plane wave is always cut-on, the incident wave is expected to be almost completely transmitted in all cases. Predictions using the finite-element analysis show the transmitted wave down less than 0.1 dB from the incident wave over the range of plane wave cases shown. The experimental data show a maximum suppression of 0.6 dB for $ka=3.68$. Consistent experimental results are shown for the plane wave over a range of frequencies and sound pressure levels. In addition, the phase response of the system is compared and shows a maximum deviation from the prediction of 18 deg.

Predictions of highly cut-on azimuthal modes (1,0) and (2,0) also showed these same transmission characteristics with a maximum suppression of 0.2 dB through the constriction geometry. The experimental data showed a range of suppressions from zero to 2.7 dB and deviations of 50 deg in the transmitted wave phase. These results reflect an increased uncertainty on the measurements and analysis with increasing

Table 2 Comparison of dominant mode amplitude and phase at the two measurement stations

Dominant mode	ka	Incident SPL	Reflected SPL	Transmitted SPL	Transmitted – Incident wave phase	
					Measured	Predicted
(0,0)	1.40	128.7	110.4	128.4	76.2	81.5
	1.40	123.9	105.3	124.0	76.2	81.5
	1.40	119.2	100.6	119.2	76.4	81.5
(0,0)	1.97	126.6	95.7	126.3	47.1	47.5
	2.51	130.8	109.9	130.4	−7.7	1.4
	3.68	123.8	103.1	123.2	298.3	316.3
(1,0)	3.84	128.9	106.9	127.3	316.7	333.8
	5.04	128.3	95.5	128.3	43.1	82.0
(2,0)	5.00	130.3	98.1	127.6	82.2	132.6
	6.25	130.2	98.2	132.2	−27.9	24.5

frequency and modal unknowns, but imply the bounds over which consistent results may be expected.

Analysis

The details of the constriction geometry were discussed earlier with the aid of Fig. 2 and Eq. (1) which defines the wall contour. For the finite-element math model section B ($x = 10.09a$) was taken as the source pressure definition plane. The termination plane occurs at $x = 11.62a$.

Acoustic Equations

The linear acoustic equations, governing the propagation of sound in an axisymmetric duct, are derived from the basic fluid mechanics relations in Ref. 6. For the case of zero mean flow, these equations simplify as follows.

$$\frac{\partial u}{\partial t} + \frac{1}{\rho_0}\frac{\partial p}{\partial x} = 0 \tag{9a}$$

$$\frac{\partial v}{\partial t} + \frac{1}{\rho_0}\frac{\partial p}{\partial r} = 0 \tag{9b}$$

$$\frac{\partial w}{\partial t} + \frac{m}{\rho_0 r}p = 0 \tag{9c}$$

$$\frac{\partial p}{\partial t} + \rho_0 c_0^2\left(\frac{\partial u}{\partial x} + \frac{\partial v}{\partial r} + \frac{m}{r}w\right) = 0 \tag{9d}$$

where the various parameters are defined in the Nomenclature. Steady-state time variations of the exp $[-j\omega t]$ type are assumed for the acoustic variables (u, v, w, p).

Boundary Conditions

The following boundary conditions are assumed.

Contour Wall:

$$\frac{\partial p}{\partial n} = 0 \tag{10}$$

Source Plane:

$$p(r,x) = \sum_n B_n J_m(\lambda_{mn} r)\, e^{j\phi_n} \tag{11}$$

Termination Plane:

$$p = \rho_0 c_0 \zeta_T u \tag{12}$$

Equation (10) represents the usual hardwall boundary condition, where $\partial(\ )/\partial n$ indicates a normal deviative with respect to the wall contour. The source plane pressure (Eq. 11) is assumed to be the superposition of one or more hardwall duct modes. B_n and ϕ_n are the mode amplitude and phase, respectively, and λ_{mn} the appropriate hardwall eigenvalue. This boundary condition does not result in any loss of generality for single propagating modes since scattering can occur only into cut-off modes for the cases presented. Also, Eq. (11) may represent a linear combination of incident and reflected waves defined at this boundary.

An impedance condition is assumed at the termination plane (Eq. 12). Here ζ_T calculated from

$$\frac{1}{\zeta_T} = \left(1 - \frac{1}{\xi^2}\right)^{1/2} \tag{13}$$

where ξ is the mode cut-off ratio (the mode propagates only if $\xi > 1.0$). Theoretically, the value of ζ_T given by Eq. (12) produces a nonreflective termination boundary condition for a single propagating mode.

Finite-Element Analysis

Details of the Galerkin/weighted-residual finite-element modeling are developed in Ref. 6. The discretization scheme is based on a quadrilateral array and utilizes a linear rectangular element. The same shape functions are used to transform the coordinate geometry as are used to describe the acoustic variables, and thus the element is isoparametric. In the transformed space the element is rectangular and this maps to a quadrilateral element in the physical space (see Ref. 6). At each mode the unknowns are (u, v, w, p) so that each element possesses 16 degrees of freedom.

All elements are assembled into a global matrix framework. Boundary conditions are satisfied by constraining nodal variables to satisfy the appropriate boundary relation [Eqs. (10-12)]. The resulting system of linear equations possesses a block tridiagonal form. A solution is achieved by forward/backward substitution following an LU decomposition.[6]

Convergence was examined by varying the number of axial and lateral elements. Acceptable results were achieved, for the frequency range of interest, by using 400 axial elements and 20 lateral elements. All finite-element calculations presented in this paper are based upon this spatial discretization.

Mode Decomposition

In order to compare the finite-element results to the experiment, a Fourier-Bessel transform similar to Eq. (5) was performed at two pairs of axial locations of the calculated solution. The reference location for each pair corresponds to planes B and D of Fig. 2 with the separation between data plane pairs of 2.44 cm at each location. The effect of this separation distance on the forward-backward wave decomposition was investigated and found to have minimal effect on the modal coefficients for the incident and reflected waves of radial modes considered.

Results and Discussion

As discussed previously, excellent agreement between the experiment and theory was shown in Table 2 for the propagation of plane waves through the constriction. Due to the nature of the plane wave mode and this excellent agreement, it was used periodically throughout the course of the experiment to provide a check on the consistency of the measurements. These checks were quite repeatable and demonstrate the stability of the experimental setup.

The primary results of this work are the comparisons between theory and experiment of the pressure reflection and transmission coefficients presented in Figs. 6 and 7 for higher-order spinning modes. These coefficients are defined in the conventional way, with the pressure reflection coefficient corrected in phase to a reference plane at $x = -5a$ or the beginning of the variable area geometry. The phase of the pressure transmission coefficient is corrected to correspond to that which would be measured over the length of the constricted section only (from $x = -5a$ to $x = +5a$ of Fig. 2).

A comparison of the measured vs calculated pressure reflection and transmission coefficients for the first azimuthal mode order (1,0) is shown in Fig. 6. The modulus of both the pressure transmission and reflection coefficients are plotted vs frequency parameter *ka*. The values for these coefficients, as obtained from the finite-element solution, balance the energy conservation relations to within 1%. The experimental trend agrees well with the theory, and except where signal-to-noise ratio problems existed (i.e., low values of pressure transmission or reflection), the amplitudes correspond within 2 dB. Note that the (1,0) mode cut-on condition at the throat diameter occurs at a *ka* value of 2.6. A comparison of the phase of pressure reflection and transmission coefficient is also shown in Fig. 6. Here the agreement between theory and experiment is quite good, being within ±20 deg, except where the transmitted or reflected acoustic field is greater than 20 dB below the incident acoustic field. This agreement implies that the finite-element algorithm is doing a good job of calculating the reflected and transmitted acoustic fields.

This same comparison is presented in Fig. 7 for the (2,0) mode. Here again the experiment has the same trend as the theory, but in absolute value does not agree as well as in the previous case. The modulus of the pressure transmission coefficients correspond within 2 dB over the frequency range considered. The pressure reflection coefficient deviates significantly at *ka* values of 3.72 and 4.00, where the deviations are −3.5 dB and −5.2 dB, respectively. The accuracy of these two points should rightfully be questioned. However, repeat cases, as will be discussed, provide similar results. A comparison of the phase results for the (2,0) mode is also plotted in Fig. 7. Here the experimentally determined values of both reflection and transmission coefficients seem to lag the finite-element results by about 70 deg across the range of *ka* values. Without this apparent shift in phase, the agreement between theory and experiment for this (2,0) mode would approximate that found in the (1,0) mode case. Note also that the (2,0) mode cut-on at the throat occurs at a *ka* value of 4.36.

With the cases near cut-on, where high reflections occur, the axial wavelength can be of the order of several meters. Some concern existed that the phase between microphones at sections A and B could not be resolved adequately since these microphones are separated by only 6.35 cm. This spacing gives only a 22-deg phase difference for the (1,0) mode at $ka = 2.0$. In order to investigate this effect, this spacing was increased to 12.06 cm and the cases near mode cut-on were repeated for both the (1,0) and (2.0) modes. These results agreed with the original results to well within 1 dB in amplitude and 10 deg in phase in all of the cases examined.

The fact that the data repeated closely and that both the pressure transmission and reflection coefficient amplitudes seem to converge to 0.9 rather than the calculated value of unity indicates some sort of systematic error is occurring. This can also be inferred from the uniform phase shift in the comparison of the (2,0) mode data. In order to discount wall dissipative effects, an effective boundary impedance was added to the propagation model to simulate acoustic boundary-layer effects. Results indicate that no significant losses occur for the limiting cases of modes near cut-on and modes

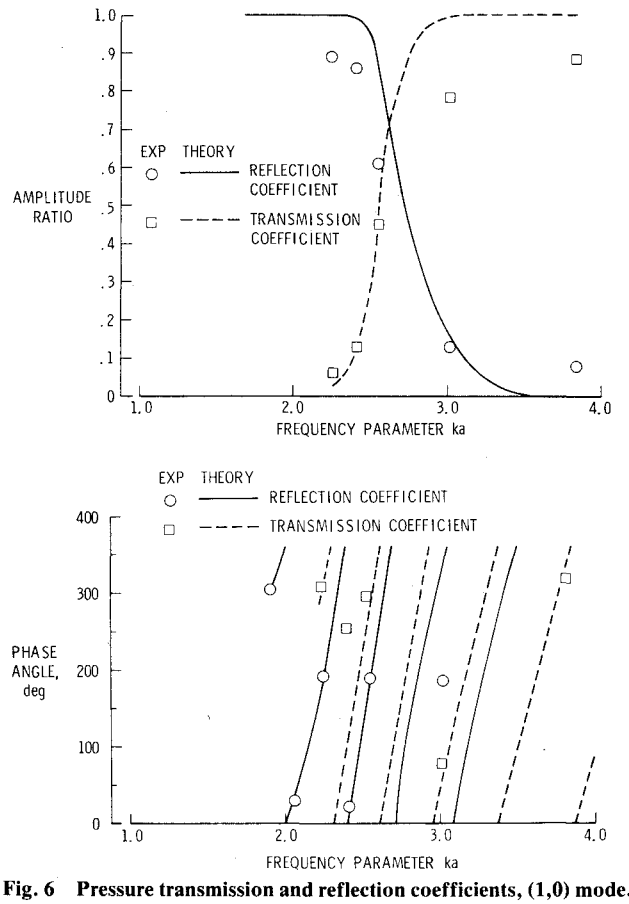

Fig. 6 Pressure transmission and reflection coefficients, (1,0) mode.

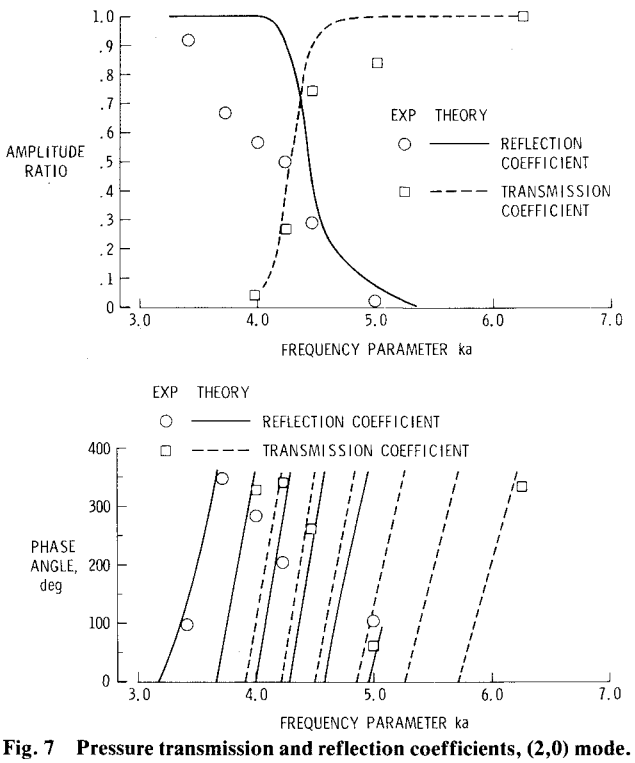

Fig. 7 Pressure transmission and reflection coefficients, (2,0) mode.

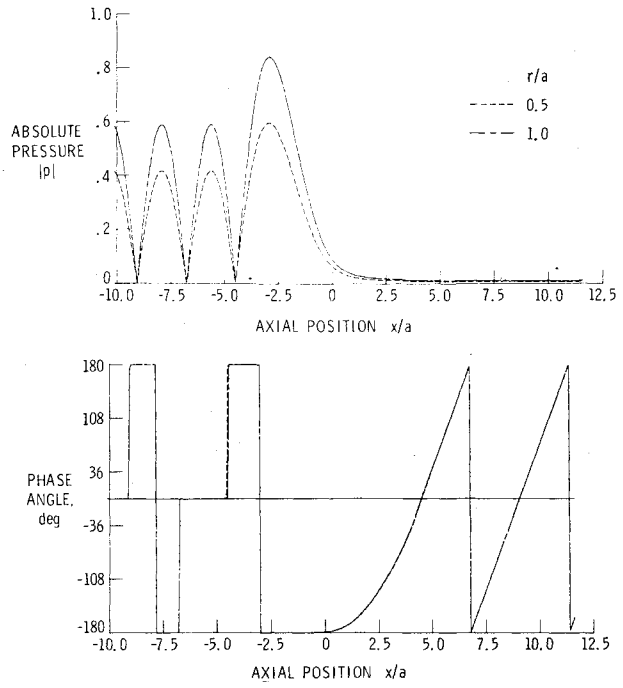

Fig. 8 Calculated axial pressure distribution for a (1,0) mode near cut-on, $ka = 2.30$.

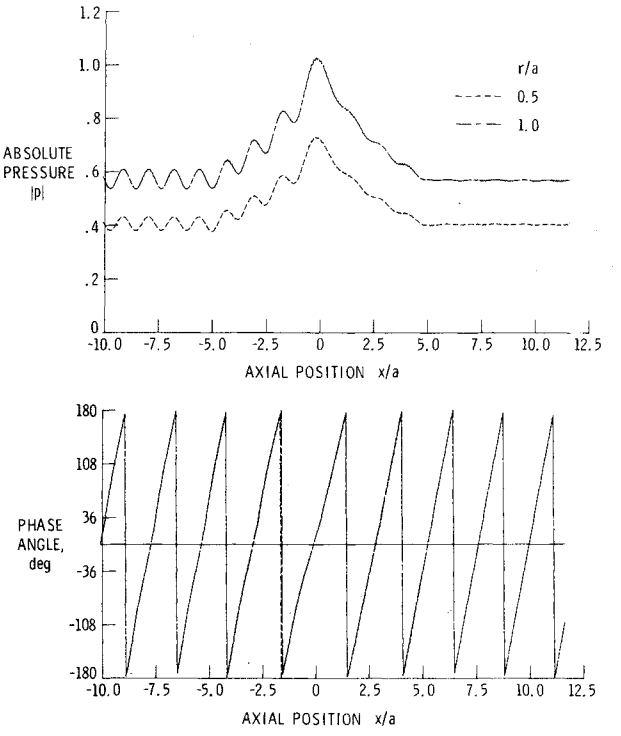

Fig. 9 Calculated axial pressure distribution for a (1,0) mode well above cut-on, $ka = 3.25$.

well away from cut-on. Other possible sources of error considered include microphone system calibration errors, biasing of the in-duct pressure measurement, and a spatial variation of the temperature inside the duct. Investigations of other possible effects will continue, but the results as presented are considered valid.

In both cases of the higher-order modes, the results imply that transmission of a particular duct mode through a constricted duct region is governed by mode cut-on at the throat diameter. The constriction essentially "turns on" over a very limited range of ka where the acoustic wave transitions very rapidly from being reflected to being transmitted. It should be noted that the theory predicts that the value of ka where equal energy is transmitted and reflected corresponds almost exactly to the respective mode throat cut-on condition. While the experimental results are not as nearly obvious, the simple concept of the modal energy switching to full transmission at the throat cut-on condition may be useful in restricting the range of mode cut-off ratios for which acoustic liners must be designed.

Figure 8 presents the calculated axial pressure distribution, amplitude, and phase for a (1,0) mode below the throat cut-on condition. In this case $ka = 2.303$ and 99.8% of the incident acoustic energy is reflected back to the source. An almost perfect standing wave pattern is noted in the figure, but with an intensification of the pressure within the constricted section itself, as would be expected. Results of this type indicate that the plane of reflection moves toward the throat as the throat cut-on condition is approached. This can be inferred from the location of the first maximum from the throat approaching the throat as ka is increased. The little transmitted energy remaining propagates in the (1,0) mode as indicated by the axial wavelength shown on the phase plot. The pressure wave itself seems to retain its identity as a (1,0) mode even in the variable area since the ratio of pressures at the wall and half-radius remains constant and the pressure at the centerline is always zero. Note also that the wall and half-radius pressure always remain in phase.

A calculation for the same mode well above cut-on, $ka = 3.5$, is presented in Fig. 9. Here, the bulk of the acoustic energy is transmitted with a pressure transmission coefficient modulus of 0.998 and a reflection coefficient of 0.06. A low amplitude standing wave is observable due to the reflection and the acoustic intensification is maximum at the throat. Again, the ratio of pressure amplitudes are constant through the constriction for the wall and half-radius values. The acoustic wavelength from the phase calculation shows a significant lengthening in the variable area section. This implies that the mode cut-off ratio is decreasing as is expected since the frequency is constant and the radius is getting smaller.

Concluding Remarks

An experiment was conducted in the NASA Langley spinning mode synthesizer to study the propagation characteristics of sound through a variable area duct section without flow. Measured pressure data were resolved on a model basis on each side of the constricted test section for $m = 1$ and 2 spinning mode sources. Measured acoustic pressure transmission and reflection coefficients were compared with finite-element computations. In general, good agreement between experiment and theory was obtained although some discrepancies were noted.

The study suggests that modal transmission through a variable area duct is governed by the throat modal cut-off ratio. Below cut-on the mode is appreciably reflected by the constricted section, whereas above cut-on the mode propagates with increasing facility through the constriction. The transition of an acoustic mode through this cut-on condition occurs over a very narrow frequency range.

The measurement and analysis techniques described herein have been shown to provide consistent results. This approach should provide a state-of-the-art basis for studying the propagation characteristics of acoustic modes under the more general condition of mean flows.

References

[1] Cho, Y. C. and Ingard, K. U., "Higher Order Mode Propagation in Nonuniform Circular Ducts," NASA TM 81481, June, 1980.

[2] Tam, C. K. W., "Transmission of Spinning Acoustic Modes in a Slightly Nonuniform Duct," *Journal of Sound and Vibration,* Vol. 18, No. 3, 1971, pp. 339-351.

[3] Eversman, W., "Multimodal Solution for Transmission of Sound in Nonuniform Ducts," AIAA Paper 76-497, 1976.

[4] Nayfeh, A. H., Kaiser, J. E., and Shaker, B. S., "A Wave Envelope Analysis of Sound Propagation in Nonuniform Circular Ducts with Compressible Mean Flows," NASA CR-3109, 1979.

[5] Sigman, R. K., Majjigi, R. K., and Zinn, B. T., "Determination of Turbofan Inlet Acoustics Using Finite Elements," *AIAA Journal*, Vol. 16, Nov. 1978, pp. 1139-1145.

[6] Abrahamson, A. L., "A Finite Element Algorithm for Sound Propagation in Axisymmetric Ducts Containing Compressible Mean Flow," AIAA Paper 77-1301, Oct. 1977; also available as NASA CR-145209.

[7] Quinn, D. W., "A Finite Difference Method for Computing Sound Propagation in Nonuniform Ducts," AIAA Paper 75-130, Jan. 1975.

[8] Nayfeh, A. H., Kaiser, J. E., Marshall, R. L., and Hurst, C. J., "A Comparison of Experiment and Theory for Sound Propagation in Variable Area Ducts," *Journal of Sound and Vibration*, Vol. 71, No. 2, 1980, pp. 241-259.

[9] Baumeister, K. J., "Numerical Techniques in Linear Duct Acoustics—A Status Report," ASME Winter Annual Meeting, Chicago, Ill., Paper 80-WA/NC-2, Nov. 16-21, 1980.

[10] Ville, J.-M. and Silcox, R. J., "Experimental Investigation of the Radiation of Sound from an Unflanged Duct and a Bellmouth, Including the Flow Effect," NASA TP-1697, Aug. 1980.

[11] Moore, C. J., "Measurement of Radial and Circumferential Modes in Annular and Circular Fan Ducts," *Journal of Sound and Vibration*, Vol. 62, No. 2, 1979, pp. 235-256.

[12] Kraft, R. E., Motsinger, R. E., Gauden, W. H., and Link, J. F., "Analysis, Design and Test of Acoustic Treatment in a Laboratory Inlet Duct," NASA CR-3161, July 1979.

[13] *NASA Langley Research Center Computer Programming Manual*, Vol. II, Sec. F5.2, Jan. 1, 1975.

[14] Golub, G. H. and Reinsch, C., "Singular Value Decomposition and Least Squares Solutions," Stanford University Rept. SV-CS-133, May 1969 (available NTIS).